Acta Cryst. (1987). A43, 418-425

X-ray Study of Planar Defects in Highly Oriented Pyrolytic Graphite (HOPG)

BY X. B. KAN, M. E. MISENHEIMER,* K. FORSTER AND S. C. MOSS

Physics Department, University of Houston, Houston, TX 77004, USA

(*Received* 2 *September* 1986; *accepted* 2 *December* 1986)

Abstract

A detailed X-ray study of HOPG reveals extensive wings on the 00.*l* Bragg reflections whose width in a scan normal to 00.*l* is comparable to the mosaic spread. These wings, which are absent in single-crystal profiles, are attributed to rotational or twist (*T*) defects between perfect substacks of pyrolyzed graphite. Along 11.*l*, the twists destroy coherence and produce an effective 'particle-size' broadening. The average substack size, or spacing between *T* defects, is estimated through profile fitting to be about 110 Å. The lateral extent of *T* defects is comparable to a mosaic-block size.

I. Introduction

This study originated with our observations, summarized in Fig. 1, of substantial symmetrical wings on the 00.*l* reflections both in pure HOPG and in stage 2 alkali-graphite intercalation compounds (GIC's), denoted approximately by $C_{12n}M$, where M = K, Rb, Cs and n = stage index (Dresselhaus & Dresselhaus, 1981). The scans in Fig. 1 were taken at the Cornell High Energy Synchrotron Source (CHESS) and are over comparable scattering angles, 2θ, to place them on the same instrumental basis with respect to slits. While the HOPG 30.0 reflection is extremely sharp and shows no wings, the 00.5 clearly has extensive tails along L (*hk.l* are hexagonal Miller indices, *HK.L* take on continuous values where $L = l$ at a 00.*l* Bragg peak). These wings are enhanced when a HOPG sample is intercalated - in this case to stage 2 with potassium. In the present paper we confine our attention to an analysis of the pure HOPG sample. A corresponding analysis of intercalated samples is in preparation.

As Moore (1973) discusses in his review of the structure and properties of pyrolytic graphite, graphite prepared by pyrolysis comes in varying degrees of perfection and has been studied and characterized rather extensively. Since Warren (1941) began with a random-layer lattice model for truly disordered (turbostratic) carbon, graphites have been shown to possess increasing degrees of stacking order with increasingly extended layer dimensions as their perfection increases. Particularly important in the X-ray treatments are the papers of Franklin (1951) and the summary of Maire & Méring (1970) who give an excellent discussion of the diffraction effects to be expected in the graphitization of soft carbons.

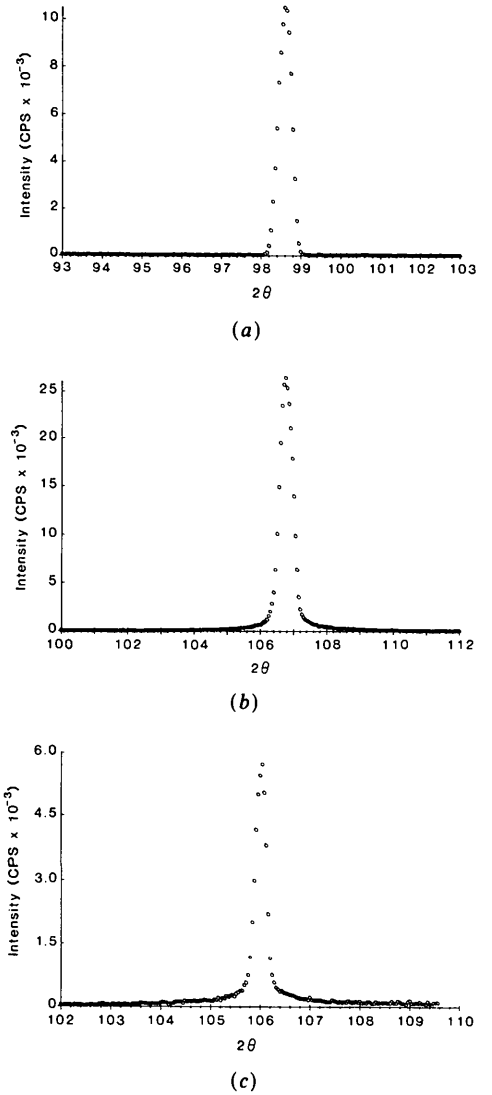

Fig. 1. Bragg reflection profiles taken at the Cornell High Energy Synchrotron Source (CHESS) on HOPG (*a*) and (*b*) and HOPG intercalated to $C_{24}K$ (*c*). Note the extensive wings on the 00.*l* reflections, (*b*) and (*c*), that are absent on *h*0.0, (*a*).

* Present address: Tracor Northern, Middleton, WI 53652, USA.

0108-7673/87/030418-08$01.50

The sequence of structures that emerges from the work of Warren (1941), Biscoe & Warren (1942), Franklin (1951), Bacon (1951), Ergun (1968) and Maire & Méring (1970) includes the following: The most disordered samples are rotationally and/or translationally uncorrelated and consist of randomly stacked hexagonal graphite net planes of quite limited lateral extent. As the order increases with the temperature of preparation, the layers become larger and orient to form substacks of coherently diffracting graphite which are separated by random rotations. Each crystal block in a pyrolytic graphite mosaic distribution is composed of these substacks. The layer spacing of the oriented material within a substack is 3·354 Å while the spacing between completely disoriented layers (as in turbostratic carbon) is 3·44 Å. As the graphitization becomes more complete, the frequency of occurrence of a spacing of 3·44 Å considerably diminishes and the substack size increases along L.

Actually, however, as the graphites become more perfect the existence of only two layer spacings becomes more problematical. Maire & Méring (1970) note that a rotationally disoriented layer, possessing a spacing different from the ideal, comes about from interstitial carbon atoms protruding into the van der Waals gap of the pyrolyzed graphite. If both layers contain these protruding carbons in sufficient numbers, the spacing will be 3·44 Å; if only one does, the spacing will be (3·44 Å + 3·354 Å)/2; and if neither contains them, the spacing will be 3·354 Å. This picture is further modified by Maire & Méring (1970) by placing distribution functions about the two expanded spacings.

As the graphitization improves, the frequency of occurrence of layers with discrete expanded spacings decreases dramatically. However, it still remains useful to consider well oriented graphite, prepared by pyrolysis, as composed of coherent substacks of large lateral extent, distributed along the common c axis with small random twists. These twists, or T defects as they are called by Maire & Méring (1970), arise, as noted, because of the existence of layers with protruding or interstitial carbon atoms. If the lateral (planar) extent of the oriented substacks is large, even a small twist will act to destroy correlations across the boundary between substacks along the c axis.

In diffraction terms, this loss of correlation means that the T defects will effectively broaden the scattering function along L for $hk.l$ reflections in exactly the same fashion as a distribution of small (flat) particles and it will be identical for every $hk.l$ point. For the $00.l$ reflections, however, the diffraction effects are basically those from a layer lattice with a distribution of one-dimensional errors in spacing. The paper of Hendricks & Teller (1942) is quite useful in analyzing such situations and has been extensively applied by Franklin (1951), Bacon (1951) and Maire & Méring (1970). The result for the $00.L$ scans is the loss of δ-function Bragg reflections which are replaced by a continuous scattering function which peaks roughly at the nominal reciprocal-lattice points ($L = l$) but whose 'breadth' increases with increasing l. When the defect density and spacing variation are both quite small, the peaks tend to look like Bragg reflections with extended tails, as in Fig. 1.

II. Experimental results

Fig. 1 shows the basic qualitative features of the $00.L$ wings that we wish to analyze: namely, that they are essentially symmetrical, that they are not present in $hk.0$ scans, and that they are enhanced on intercalation. Because intercalation also introduces staging disorder (Misenheimer & Zabel, 1985), we defer discussion of Fig. 1(c) to a later date. Fig. 2 presents data taken in our laboratory using a sealed (Cu) tube diffractometer operated at a maximum of 40 kV and 30 mA with a pre-sample curved Ge(111) asymmetrically cut Johannson monochromator. The monochromator–slit arrangement gave us a symmetrical Cu $K\alpha_1$ incident beam with a narrow combined incident–diffracted beam divergence of ~0·05° in θ as measured at 11.0. Fig. 2(a) is an uncorrected (raw)

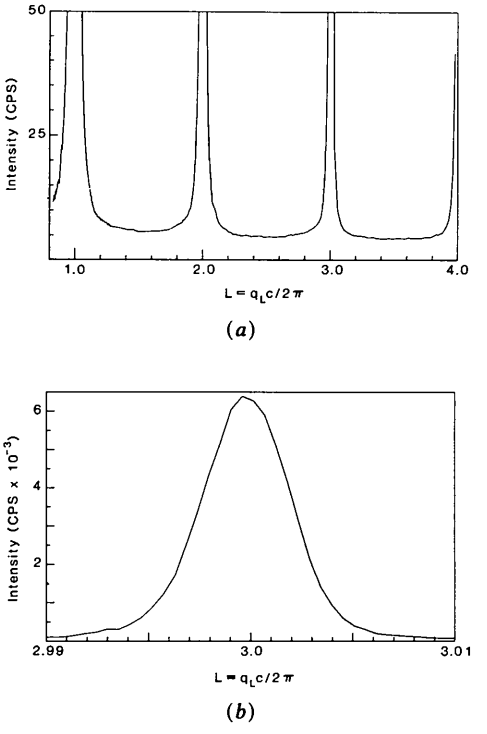

Fig. 2. (a) Laboratory (sealed tube) Cu $K\alpha_1$ X-ray scan along L through several $00.l$ reflections from HOPG where $\mathbf{q}_L = \mathbf{q}$, the diffraction vector whose magnitude $|\mathbf{q}_L| = 4\pi \sin\theta/\lambda$, and c = 3·354 Å. (b) Detailed 00.3 profile, taken on a laboratory source as in (a), showing a narrow peak and no Cu $K\alpha_2$ line.

00.L scan in which the shape of the Bragg profiles over a large scan range is shown. (The l index in these scans refers to $1/c$ where $c \simeq 3{\cdot}354$ Å. For the normal AB stacking of graphite, c is actually $2\times 3{\cdot}354$ Å and this spacing is used on $hk.l$ indexing.) Without further analysis one might be tempted to assign the profile in Fig. 2(a) to thermal diffuse scattering (TDS), although for graphite that is unlikely because of the high Debye temperatures for both c-axis and basal plane vibrations (Chen & Trucano, 1978). Fig. 2(b) presents the 00.3 Bragg profile to emphasize the essentially symmetrical character of the reflection and its narrow width. If we take the full width at half maximum (FWHM = $\Delta q_{1/2}$) of this reflection we see that it is nearly resolution limited [$\Delta q_{1/2} = (2\pi/c)\Delta L_{1/2} = 0{\cdot}009$ Å^{-1}]. The coherent particle size along the c axis, determined from such a 00.l width, is thus extremely large when the instrumental width is removed.

Fig. 3 presents ω scans of the HOPG 00.3 reflection and the 00.2 reflection of a graphite single crystal that we shall use for comparison. Fig. 3(a) indicates a mosaic spread of about 0·5° FWHM for our HOPG sample, which was supplied by Dr A. W. Moore. The natural graphite crystal, provided by Dr C. J. Sparks, shows basically two narrow distributions, each of about 0·1–0·2° width and sitting on a broader distribution whose entire spread is of order 1°.

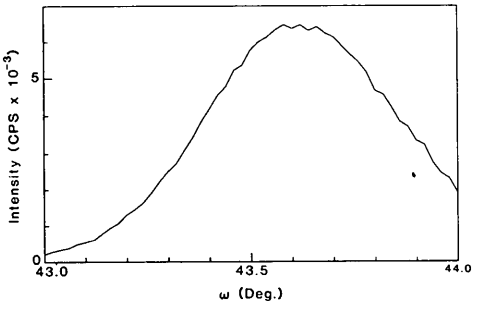

(a)

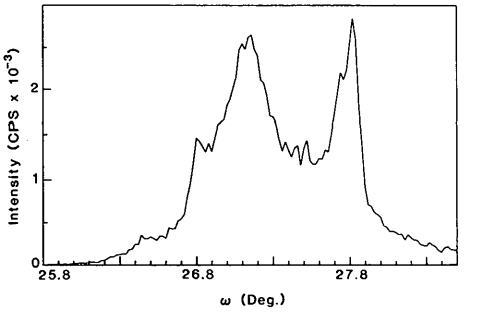

(b)

Fig. 3. (a) ω scan of the HOPG 00.3 reflection showing a FWHM of about 0·5°; the cut-off at large ω was inadvertent but the profile is smooth over the whole range. (b) ω scan of the 00.2 reflection from a natural graphite single-crystal flake.

Fig. 4 compares these two samples in what is referred to as an HK scan. For HOPG this entails scanning at fixed L ($\neq l$) in a direction normal to the c direction. Because HOPG is cylindrically averaged about c, the notation 'HK' is used. The units are such that $HK = 1{\cdot}0$ when the diffraction vector touches the 10.L rod at any value of L. Fig. 4(a) shows that the wing of the Bragg peak near 00.1 is really a narrow ridge of intensity sitting on a background of TDS and Compton scattering. To facilitate our analysis of this ridge, we made a polynomial fit to the background and that is shown as the solid line in Fig. 4(a). The extent of the ridges in HK, normal to $\mathbf{c}^*$, is essentially given by the mosaic spread. The comparable single-crystal HK scan in Fig. 4(b) has a background fit by the same polynomial as Fig. 4(a) and there is clearly no ridge. This result establishes the pronounced wings in HOPG along an L scan as due to defects peculiar to HOPG which are absent in the natural single crystal. Because the wings are really narrow ridges, the lateral extent of the defects is comparable to the lateral dimension of the layers in a diffracting block or substack.

Fig. 5 presents a series of HK scans at various values of L showing that the ridge remains narrow, normal to $\mathbf{c}^*$, as the intensity falls off. Estimating

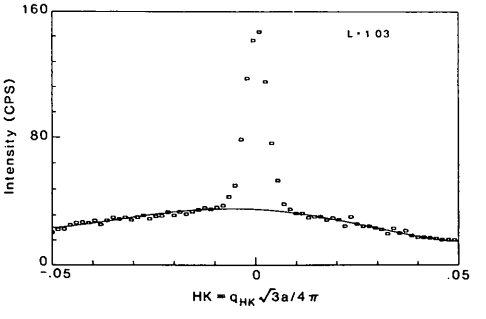

(a)

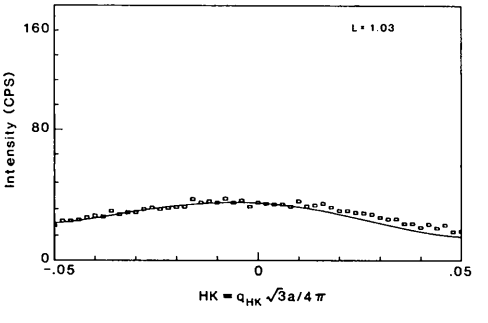

(b)

Fig. 4. HK scans normal to the c^* direction at $L = 1{\cdot}03$, where $\mathbf{q}_{HK} + \mathbf{q}_L = \mathbf{q}$ and $q_{HK}^2 + q_L^2 = q^2 = (4\pi \sin\theta/\lambda)^2$: ($a$) HOPG, showing a ridge on top of the thermal and Compton background. (b) Single crystal (of Fig. 3b) showing no ridge. The solid curve is identical for both and is a polynomial fit to the background in (a) which is applied to (b).

background at $L=1{\cdot}10$ and $L=1{\cdot}15$ becomes increasingly difficult and the polynomial fits at these two L values are probably in error. (At $L=1{\cdot}10$ the background rises in an unphysical way at $HK=0$. We have not corrected for this, however, leaving all background estimates as systematically determined.)

Fig. 6 shows L scans for the 11.2 and 11.4 reflections together with, in Fig. 6(a), a theoretical profile to be discussed and, in Figs. 6(a) and 6(b), theoretical total fits involving a convolution of the theoretical profile with the experimentally determined instrumental broadening. While we defer detailed comment on these to the next section, two experimental aspects are noteworthy. The first is that scans along L at 11.l will contain a broadening contribution due to the mosaic spread of the sample. For example, at 11.0 an L scan is nearly identical to an ω scan. One must be quite careful, therefore, in assigning crystallite dimensions to L scans. The second point to be noted is that, given the above caution, these 11.l profiles remain considerably broader than the comparable 00.l profiles. It is this fact which is essential in the assignment of a model for HOPG in which we have one-dimensional disorder along 00.L, characterized by the spacing error(s) introduced by the T defects; along 11.L, on the other hand, we have profiles determined by the average dimension of the coherently diffracting substacks between the T defects which, by their nature, destroy coherence along L for $hk.l$ reflections.

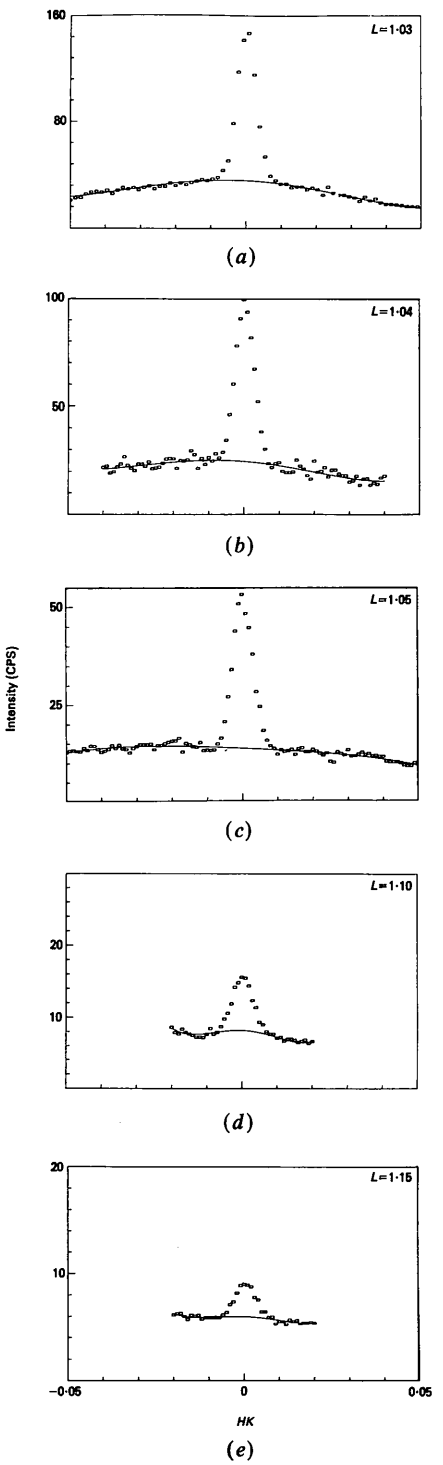

Fig. 5. HOPG HK scans at selected values of L near the 00.1 reflection showing the ridge of diffuse intensity above the fitted background (solid curves).

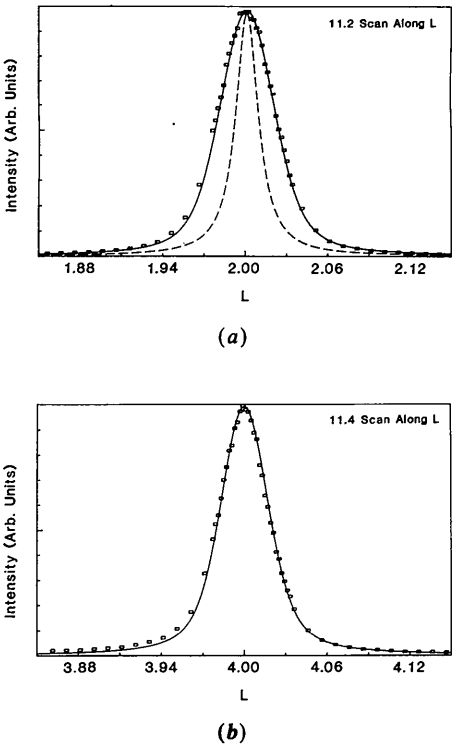

Fig. 6. Scans at 11.2 and 11.4 along L in which the squares are data points and the solid curves are a fit to theory, shown as a dashed curve at 11.2, convoluted with the instrumental profile as described in the text.

III. Theory and data analysis

As the T defect is a one-dimensional defect, the Hendricks–Teller (1942) theory is well suited to our purpose. Graphite also contains stacking faults which give rise to L-dependent broadening in $hk.L$ bands with $h-k \neq 3m$, but which have no effect on the $00.L$ and $hk.L$ ($h-k=3m$) bands. We therefore concentrate on $00.L$ and $11.L$ bands in order to avoid the difficulty of distinguishing the influence of T defects from stacking-fault effects.

A. $00.L$ band

The intensity per layer as given by Hendricks & Teller (1942) is

$$I_N(S)/N = 1/N \sum_{n=0}^{N-1} \sum_{m=0}^{N-1} \langle f_0 f_0^* \exp[i(\varphi_n - \varphi_m)]\rangle, \quad (1)$$

where N is the total number of layers, f_0 is the layer form factor, which is a multple of the atomic form factor for carbon, and φ_n is the phase factor of the nth layer: $\varphi_n = 2\pi S x_n$ with $S = 2\sin\theta/\lambda$, and x_n is equal to the distance between the nth and oth layers.

We assume that the T defects are distributed randomly, in which case the spacing between any pair of nearest-neighbor layers can be represented by a distribution function $h(x)$ [$\int_0^\infty h(x)\,dx = 1$]. Let $N \to \infty$; (1) then becomes

$$\begin{aligned} I_p(S) &= \lim_{N\to\infty} I_N(S)/N \\ &= f_0^2\left\{2\,\mathrm{Re}\left[\sum_{n=1}^{\infty}\langle\exp(i\varphi_n)\rangle\right]+1\right\} \\ &= f_0^2\left\{2\,\mathrm{Re}\left[\sum_{n=1}^{\infty}\langle\exp(i\varphi_1)\rangle^n\right]+1\right\} \\ &= f_0^2(2\,\mathrm{Re}\{\langle\exp(i\varphi_1)\rangle/[1-\langle\exp(i\varphi_1)\rangle]\}+1) \\ &= f_0^2[1-\rho^2(S)]/[1+\rho^2(S)-2\rho(S)\cos\varphi(S)] \end{aligned} \quad (2)$$

where

$$\rho(S)\exp[i\varphi(S)] = \langle\exp(i\varphi_1)\rangle = \int_{-\infty}^{\infty}\exp(i2\pi Sx)h(x)\,dx \quad (3)$$

and $\rho(S)$, $\varphi(S)$ are real.

For a specific known function for $h(x)$, $\rho(S)$ and $\varphi(S)$ can be evaluated. Equation (3) can be simplified further by realizing that the spacing associated with a T defect is only slightly larger than the normal c-axis interplanar spacing, and we can therefore expand (3). Let $\bar{x} = \int_{-\infty}^{\infty} xh(x)\,dx$, $\delta^2 = \int_{-\infty}^{\infty}(x-\bar{x})^2 h(x)\,dx$. Then

$$\begin{aligned} &\int_{-\infty}^{\infty}\exp(i2\pi Sx)h(x)\,dx \\ &\quad = \exp(i2\pi S\bar{x})\int_{-\infty}^{\infty}\exp[i2\pi S(x-\bar{x})]h(x)\,dx \\ &\quad \simeq \exp(i2\pi S\bar{x})\left\{1-\tfrac{1}{2}\int_{-\infty}^{\infty}[2\pi S(x-\bar{x})]^2 h(x)\,dx\right\} \\ &\quad \simeq \exp(i2\pi S\bar{x} - 2\pi^2 S^2\delta^2). \end{aligned}$$

$\rho(S)$ now takes on the simple form $\rho(S) = \exp(-2\pi^2 S^2\delta^2)$, $\varphi(S) = 2\pi S\bar{x}$. The final intensity formula used to fit our data can then be written as

$$I(S) = CAP\,\mathrm{LF}\exp(-2M)f_C^2 \times[1-\rho^2(S)]/[1+\rho^2(S)-2\rho(S)\cos\varphi(S)], \quad (4)$$

where C is a scaling constant, A is the absorption factor $= 1-\exp(-2\mu t/\sin\theta)$, P is the polarization factor $= 1+\cos^2 2\theta\cos^2 2\theta_m$, θ_m = monochromator angle, $\exp(-2M)$ is the Debye–Waller factor (Chen & Trucano, 1978), f_C is the carbon scattering factor (*International Tables for X-ray Crystallography*, 1974), and LF is the Lorentz factor.

For the absorption coefficient, μt was experimentally determined. In order to subtract the background (TDS + Compton) before a comparison with (4) could be made, we took a set of HK scans across a $00.L$ band, as indicated in Fig. 5, from which we obtained two related sets of data: (a) the peak height of the ridge above background, and (b) the area under the ridge above the background; these are shown in Fig. 7.

The combined Lorentz factor and slit function along L for this sample was difficult to evaluate exactly. The scattering is diffuse along L but confined to the mosaic ridge and both horizontal- and vertical-divergence corrections are necessary along with the true Lorentz factor. [None of these is necessary for thermal diffuse scattering as long as it is not too sharply varying.] We found for the values of peak intensity (Fig. 7a) along L at $HK = 0$ that a simple $1/\sin 2\theta$ factor enabled us to place the data about 00.1 and 00.2 on the same scale for theoretical comparison. Because this was a rather empirical choice we also compared the integration under the ridge in Fig. 7(b). If LF in Fig. 7(a) is $1/\sin 2\theta$, the scans in Fig. 7(b), taken at constant steps in HK, will automatically have an angular (geometric) 'Lorentz factor' of $1/\cos\theta$. The agreement between the two ways of plotting the results in Fig. 7 lends credence to our initial choice.

The fits in Fig. 7 to (4) are thus identical except for the value of LF. They are placed on an absolute

scale by normalizing at one point. The only variable is the value of δ which is found by a visual best fit to be $\delta = 0{\cdot}008\ (1)$ Å ($\bar{x}$ is given by the c-lattice parameter). The very small value of δ may be compared with the c-axis root mean square amplitude of thermal vibration, $\langle\mu^2\rangle^{1/2} = (B_c/8\pi^2)^{1/2} = 0{\cdot}12$ Å, as reported by Chen & Trucano (1978). The one-dimensional static fluctuation is almost two orders of magnitude smaller than the thermal amplitude; we shall discuss its interpretation presently.

B. 11.*L band*

Since the structure inside a substack is regular, the intensity per layer from one such substack with N layers is

$$I_N(L)/N = f_0^2\left(1+2\,\mathrm{Re}\left\{\sum_{n=1}^{N-1}[(N-n)/N]\exp(iL\pi n)\right\}\right).$$

The total intensity is then the sum of the intensities from all substacks. Let α_N be the weight fraction of substacks with N layers ($\sum_{N=1}^{\infty}\alpha_N = 1$). Following a treatment similar to Maire & Méring (1970), we may write

$$I_p(L) = I_{\text{total}}(L)/N_{\text{total}} = \sum_{n=1}^{\infty}\alpha_N I_N(L)/N = f_0^2\left\{1+2\,\mathrm{Re}\left[\sum_{n=1}^{\infty}\beta_n\exp(iL\pi n)\right]\right\},$$

where

$$\beta_n = \sum_{N=n+1}^{\infty}\alpha_N(N-n)/N.$$

Let P be the probability of finding a T defect between any nearest-neighbour pair and $P_1 = 1-P$. Then

$$\alpha_N = [(1-P_1)^2/P_1]NP_1^N, \quad \beta_n = P_1^n.$$

Therefore

$$I_p(L) = f_0^2\left(1+2\,\mathrm{Re}\left\{\sum_{n=1}^{\infty}[P_1\exp(iL\pi)]^n\right\}\right) = f_0^2(1-P_1^2)/[1+P_1^2-2P_1\cos(\pi L)]. \quad (5)$$

This expression can also be found in Franklin (1951) and Bacon (1951) for the evaluation of *hk.l* profiles along L. Notice that (5) is periodic along L which means that all 11.*l* peaks have the same shape and width once the broadening due to finite instrumental resultion combined with the mosaic spread of the sample is accounted for. Fig. 8 depicts the particular experimental diffraction situation appropriate to HOPG with a modest mosaic spread. The total broadening was assumed to be Gaussian with a width determined in the following way.

First, we took radial scans across the 11.2 and 11.4 peaks and found the profiles to be essentially Gaussian. From this we obtained the radial width W_R

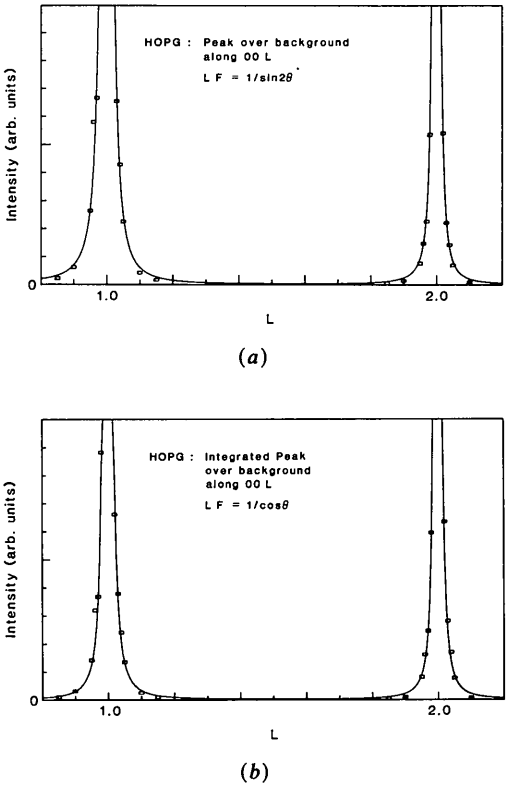

Fig. 7. Plots of data (squares) against theory (solid line) in equation (4) with the Lorentz factor LF consistently chosen to give the peak intensity (*a*) and integrated intensity (*b*) in the 00.*l* ridges above background. For the best fit $\delta = 0{\cdot}008\ (1)$ Å.

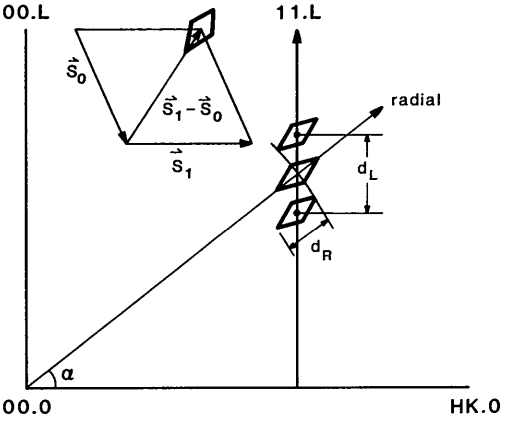

Fig. 8. Reciprocal-lattice geometry for 11.L scans incorporating both mosaic spread (denoted by the arc normal to the radial vector) and the usual volume element sketched in detail. d_R is an effective width for a radial (θ-2θ) scan which gives rise to d_L in the L scan.

of the Gaussian curve. The widths W_L in the 11.L scans are derived from W_R by noting that if there is no T defect the intensity distribution of a 11.l peak in reciprocal space is a (mosaic) arc across the central 11.l position as in Fig. 8. The small rhombi in Fig. 8 show the instrumental resolution volume projected onto the plane.

If we now take two scans - one, as above, through the 11.l peak radially, the other through the peak in the L direction - both scans will have an approximately Gaussian profile. In both scans, when the upper right corner of the rhombus touches the mosaic arc the intensity begins to build up, gradually reaching a maximum as the rhombus moves outwards, and then drops back to zero again when the lower left corner touches the arc.

The total distance travelled by the center of the rhombus during this process will be denoted as d_R or d_L in radial or 11.L scans respectively. From the geometry, it is clear that $d_L/d_R = 1/\sin\alpha$. d_L and d_R are directly related to the width of the Gaussian curves. But before we can establish a relation between the two widths, W_L and W_R, it must be noted that the intensity along the mosaic arc falls from the central point in Fig. 3(a). While both corners of the rhombus meet the arc at the central point in a radial scan, they touch the arc at positions away from this maximum in a 11.L scan. Thus the intensity drops faster in a 11.L scan than in a radial scan, and the ratio of two widths, W_L/W_R, is less than the ratio d_L/d_R. From our data we take $W_L/W_R \simeq \frac{3}{4}(d_L/d_R) = 3/(4\sin\alpha)$ in our fitting. Finally, we have $W_L = 3W_R/(4\sin\alpha)$.

After this broadening correction is determined, its convolution with (5) may be performed to compare with the peak or integrated ridge data. Fig. 6 shows the 11.2 and 11.4 experimental peaks together with the theoretical result convoluted with the broadening function. We also include the theoretical part of (5) separately in Fig. 6(a) to show its shape and relative width. The best fit, again chosen visually, is not perfect because the mosaic distribution cannot be represented so simply. But it is equally good at 11.2 and 11.4 and yields a $P_1 = 0{\cdot}97$. Thus, $P = 1 - P_1 = 0{\cdot}03$, which means that there exists one T defect in about every 33 layers and that the coherent block size may be estimated to be $33 \times 3{\cdot}35$ Å $\simeq 110\,(20)$ Å.

C. *Thermal and Compton background*

We also tried to fit the background data obtained from the same set of HK scans that were summarized in Fig. 5. The solid curve in Fig. 9 is obtained by plotting first-order TDS and Compton scattering plus an extra constant background term. The expressions we employed are:

$$I_{\text{background}} = I_{\text{TDS}_1} + I_{\text{Compton}} + \text{constant},$$

where

$$I_{\text{TDS}_1} = f_C^2 \exp(-2M) 4\pi^2 N k_B T |S|^2 PA/m_C \omega_{g,L}^2 \quad (6)$$

$$I_{\text{Compton}} = NF_c(S)PA. \quad (7)$$

P and A are polarization and absorption factors respectively and m_C is the mass of a carbon atom. In (6) the Debye-Waller factor is evaluated using the c-axis thermal parameter of Chen & Trucano (1978) and the carbon scattering factor comes, as before, from *International Tables for X-ray Crystallography* (1974). The phonon frequencies $\omega_{g,L}$ refer to the longitudinal (c-axis) vibrations where $\mathbf{g} = 2\pi\mathbf{S} \pm \mathbf{q}_L$, the phonon wave vector. The values for $\omega_{g,L}$ were obtained from Nicklow, Wakabayashi & Smith (1972).

$F_c(S)$ in (7) is from *International Tables for X-ray Crystallography* (1974). The constant-background term originates in multiple elastic and inelastic scattering becuase of the high transparency of the sample. Rather than attempt to estimate multiple scattering, we assigned a constant level to this contribution and could then obtain the satisfactory fit in Fig. 9 by fixing only one point of theory to experiment as a normalization.

IV. Discussion

We have shown that the T-defect model proposed by Maire & Méring (1970) for partially graphitized carbon remains meaningful in these highly oriented pyrolytic graphites for which the coherent block size in our particular sample is roughly 110 Å. (We would expect it to be similar in similarly treated samples.)

According to Maire & Méring (1970), each face of a graphite layer can be in either an α or a β state. The β state is that of the face of a perfect graphite layer, while the α state pertains to a face which has interstitial carbons grafted onto it. The perfectly ordered arrangement between layers is possible only for β-β contact; otherwise there is a T defect, as mentioned in the *Introduction.*

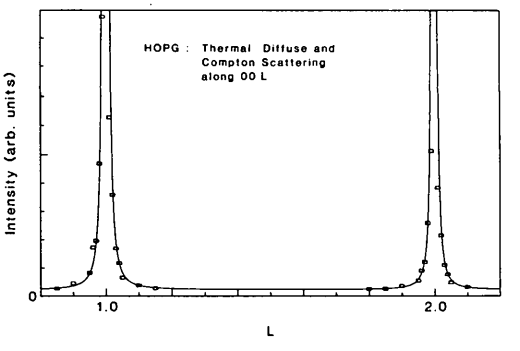

Fig. 9. Calculated (TDS + Compton) *versus* measured background scattering under the 00.L ridges, including a small constant contribution from multiple scattering.

The graphitization factor g $(=P_1)^{1/2}$ is 0·984 in our HOPG sample; this is also the probability of finding *either* face of a layer in a β state. The frequency of occurrence of β-β, α-β and α-α contact thereby becomes (Maire & Méring, 1970) g^2, $2g(1-g)$ and $(1-g)^2$ respectively, with associated spacings of 3·354, 3·397 [$=(3\cdot354+3\cdot44)/2$] and 3·44 Å, respectively. Thus the average spacing is given by $\bar{d}=3\cdot354\,g^2+3\cdot397\times2g\,(1-g)+3\cdot44\,(1-g)^2=3\cdot44-0\cdot086\,g=3\cdot355$ Å. This spacing is so close to the ideal spacing that the difference would not be detected in our experiment. If we assume that the three spacings are discrete, the variation δ^2 will be given by $\delta^2=(3\cdot354-\bar{d})^2g^2+(3\cdot397-\bar{d})^2\,2g(1-g)+(3\cdot44-\bar{d})^2(1-g)^2=0\cdot0037g(1-g)=5\cdot5\times10^{-5}$ Å^2. This agrees quite well with our experimental value of $\delta^2=(0\cdot008)^2=6\cdot4\times10^{-5}$ Å^2. On the other hand, Maire & Méring (1970) have shown the inadequacy of the above equation in the soft carbons, and therefore assume that the spacings associated with α-β and α-α contact have a continuous distribution with width δ_1 ($\delta_1^2=0\cdot17$) and δ_0 ($\delta_0^2=0\cdot06$) respectively; then $\bar{\delta^2}=g(1-g)(0\cdot0037+2\delta_1^2)+(1-g)^2\delta_0^2$. If $g=0\cdot984$, $\delta^2=5\cdot8\times10^{-4}$ Å^2 which is roughly an order of magnitude greater than the experimental value. For our nearly perfect graphite samples, a discrete spacing for the (occasional) defective layer, rather than a distributed set, seems therefore most appropriate.

The value of $\delta=0\cdot008$ Å is, as mentioned earlier, very small, being almost two orders of magnitude smaller than the c-axis root mean square thermal amplitude. Its detectability, however, with standard X-ray apparatus, is quite acceptable and provides insight into the limits available for layer-defect effects. In the intercalated sample of Fig. 1(c) the effects are more pronounced but are almost certainly complicated by stage mixing. We are therefore studying an intercalated single crystal in which T defects do not (initially) exist, in order to sort out the two contributions.

Finally, we note that HOPG is obtained by heat treatment of massive pyrolytic graphite (Moore, 1973). The starting material consists mainly of $\alpha\alpha$ layers in which both faces have protruding carbon atoms. In the process of heat treatment, the α state is transformed into a β state leading to a more ordered structure with some α states, or T defects, persisting in the final product. It is in a sense gratifying to be able to proceed with a consistent description of the structure of these synthetic graphites from the most disordered state to a more nearly perfect state in which, despite the apparent perfection of HOPG, an average substack of only ~110 Å seems to prevail in our sample.

We thank Dr A. W. Moore for our HOPG sample. Professor H. Zabel and Mr P. Chow collaborated in the collection of the data in Fig. 1 and we thank them for many discussions of these experiments. Early observations of wings in Rb-intercalated HOPG were also made by C. Thompson as part of her PhD research (in progress) at the University of Houston. This research was supported by the NSF with Grant No. DMR-8603662.

References

BACON, G. E. (1951). *Acta Cryst.* **4**, 558-561.
BISCOE, J. & WARREN, B. E. (1942). *J. Appl. Phys.* **13**, 364-371.
CHEN, R. & TRUCANO, P. (1978). *Acta Cryst.* A**34**, 979-982.
DRESSELHAUS, M. S. & DRESSELHAUS, G. (1981). *Adv. Phys.* **30**, 139-326.
ERGUN, S. (1968). *Chemistry and Physics of Carbon*, Vol. 3, pp. 211-288. New York: Marcel Dekker, Inc.
FRANKLIN, R. E. (1951). *Acta Cryst.* **4**, 253-261.
HENDRICKS, S. B. & TELLER, E. (1942). *J. Chem. Phys.* **10**, 147-167.
International Tables for X-ray Crystallography (1974). Vol. IV. Birmingham: Kynoch Press. (Present distributor D. Reidel, Dordrecht.)
MAIRE, J. & MÉRING, J. (1970). *Chemistry and Physics of Carbon*, Vol. 6, pp. 125-190. New York: Marcel Dekker, Inc.
MISENHEIMER, M. E. & ZABEL, H. (1985). *Phys. Rev. Lett.* **54**, 2521-2524.
MOORE, A. W. (1973). *Chemistry and Physics of Carbon*, Vol. 11, pp. 69-187. New York: Marcel Dekker, Inc.
NICKLOW, R., WAKABAYASHI, N. & SMITH, H. G. (1972). *Phys. Rev. B*, **5**, 4951-4962.
WARREN, B. E. (1941). *Phys. Rev.* **9**, 693-698.